

Optimization of ROI Size for Development of Computer Assisted Framework for Breast Tissue Pattern Characterization Using Digitized Screen Film Mammograms

Indrajeet Kumar*, **Jitendra Virmani[†]**, **H.S. Bhadauria[‡]**

*Galgotia Educational Institutions, Greater Noida, India, [†]CSIR-CSIO, Chandigarh, India,

[‡]GBPIET, Pauri, India

1 Introduction

Mammography, an X-ray of breast is frequently used modality for the prediction of breast lesions. Among the various breast lesions, breast tumor is the major cause for death of ladies in the developed country as well as in developing country across the world [1,2]. Breast density or breast tissue is considered as a well-built and major sign for the development of breast lesions [3–24]. Breast tissue pattern characterization is considered as the dilemma of texture analysis, because the variations in breast tissue pattern characteristics are easily predicted by the variations in textural appearance.

These days telemedicine and intelligent systems are increasingly being used in health care for automatic Prediction of diseases using biomedical signals and images generated from CT-scan, X-ray, Ultrasound, and PET scanners. The information related to design of few such systems for analysis of medical signals and images can be found in Refs. [25–33].

Developing CAD system for characterization of breast tissue patterns is clinically significant because in daily clinical practice there are so many cases found such that breast lesions are not clearly visible because of dense tissue. There might be a chance that lesions are presents but it is hidden behind the dense tissue therefore not clearly visible. So it is suggested that if the observation of such test case is dense (BIRADS-III/BIRADS-IV) then these types of cases must be go for double screening for the prediction of lesions that are hidden behind the dense tissue.

The breast imaging-reporting and data system (BIRADS) breast density definitions [3, 8–11, 14–17] and the sample mammogram of each class, taken from the digital database for screening mammography (DDSM) dataset is shown in Fig. 1.

Studies in literature indicate that there has been notable curiosity among the research community to design computer assisted characterization systems for prediction of breast density [34–60]. These computer-aided characterization/classification systems have been designed by using (a) segmented tissue based approaches (STBAs) or (b) fixed size region of interest (ROI) based approaches (RBAs). It is worth mentioning that more studies have been carried out on computer aided classification system designs using STBAs [34–38, 43, 44, 54–57, 59, 60] and the related studies on computer aided classification system designs based on RBAs are few [39–42, 45–53, 58]. It may be noted that computer aided classification system designs using STBAs require automatic segmentation of breast tissue which involves additional tasks like background elimination, pectoral muscle removal. These additional steps make STBAs more complex and time-consuming approach with respect to RBAs.

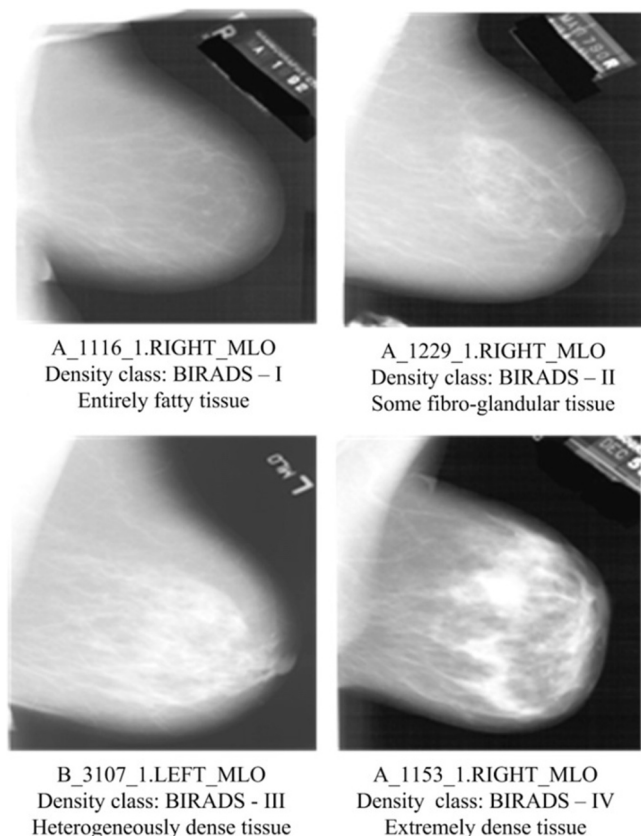


Fig. 1
Sample image of different BIRADS breast density classes.

The brief details of the related studies conducted in past for breast tissue pattern characterization are given in [Table 1](#).

From [Table 1](#), it can be concluded that the studies on breast tissue pattern characterization (4-class and 2-class) have been performed on (a) benchmark dataset or (b) set of

Table 1 Related studies for breast tissue pattern characterization

Author(s), Year	STBA/RBA	No. of Images	Considered Class			Accuracy (%)
			Class	Classifier		
Studies carried out on DDSM image dataset						
Bovis et al. 2002 [34]	STBA	377	4-Class 2-Class	ANN ANN		71.4 96.7
Oliver et al. 2005 [35]	STBA	300	4-Class	kNN		47.0
Bosch et al. 2006 [36]	STBA	500	4-Class	SVM		84.7
Oliver et al. 2008 [37]	STBA	831	4-Class	SFS-kNN		77.0
Oliver et al. 2010 [38]	STBA	831	4-Class	LDA-PCA		94.0
Kumar et al. 2015 [39]	RBA	480	4-Class	SVM		73.7
Kumar et al. 2017 [40]	RBA	480	4-Class	HHC ^a		84.6
Kumar et al. 2017 [41]	RBA	480	4-Class	ENN ^b		90.8
Kumar et al. 2018 [42]	RBA	480	4-Class 2-Class	PNN SVM		72.5 91.2
Studies carried out on MIAS image dataset						
Oliver et al. 2005 [35]	STBA	270	4-Class	Decision tree		73.0
Bosch et al. 2006 [36]	STBA	322	4-Class	SVM		95.3
Oliver et al. 2008 [37]	STBA	322	4-Class	SFS-kNN		86.0
Oliver et al. 2010 [38]	STBA	322	2-Class	kNN		94.0
Qu et al. 2011 [43]	STBA	322	4-Class	FELM ^c		72.6
Chen et al. 2011 [44]	STBA	322	4-Class 2-Class	kNN kNN		75.0 88.0
Mustra et al. 2012 [45]	RBA	322	4-Class 2-Class	SFS-kNN kNN		79.3 91.6
Sharma et al. 2014 [46]	RBA	322	2-Class	SMO-SVM		96.4
	RBA	212	2-Class	kNN		97.2

Continued

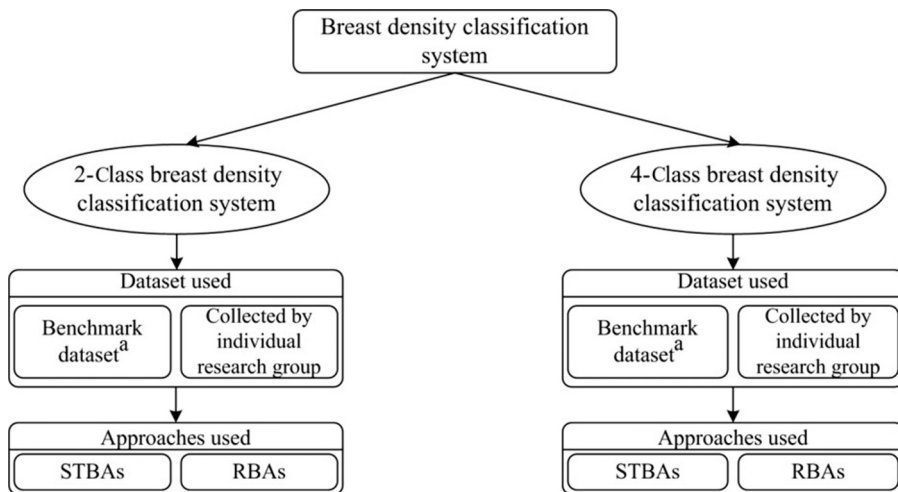
Table 1 Related studies for breast tissue pattern characterization—Cont'd

Author(s), Year	STBA/RBA	No. of Images	Considered		
			Class	Classifier	Accuracy (%)
Sharma et al. 2015 [47]	RBA	322	2-Class	kNN	96.2
Virmani et al. 2015 [48]	RBA	322	2-Class	PCA-SVM	94.4
Kriti et al. 2015 [49]	RBA	322	2-Class	PCA-ANN	95.2
Kriti et al. 2016 [51]	RBA	322	2-Class	PCA-SSVM	94.4
Kriti et al. 2017 [52]	RBA	322	2-Class	SSVM	89.4
Kriti et al. 2018 [53]	RBA	322	2-Class	ANN	93.7
Studies carried out on mammographic image dataset collected by authors					
Miller et al. 1991 [54], Karssemeijer, 1998 [55]	STBA	40	4-Class	Bayesian	80.0
Petroudi et al. 2003 [56]	STBA	615	4-Class	kNN	65.0
Jamal et al. 2007 [57]	STBA	132	2-Class	kNN	75.7
Liu et al. 2011 [58]	RBA	100	4-Class	—	78.3
Mustra et al. 2012 [45]	RBA	88	4-Class	SVM	86.4
Masmoudi et al. 2013 [59]	STBA	144	4-Class	SFS-kNN	76.4
He et al. 2016 [60]	STBA	2052	2-Class	ANN	97.2
			4-Class	kNN	79.0
			4-Class	—	78.0

^aHHC, hybrid hierarchical classifier.^bENN, ensemble of neural network.^cFELM, fuzzy extreme learning machine; 4-class classification consists of BIRADS breast density classification; 2-class classification consists of fatty and dense breast density classes.

mammographic images collected by individual research group as shown in Fig. 2. The literature studies show the development of breast density classification system as shown in Fig. 2.

Further, it can be noticed from Table 1, that STBAs based 4-class breast tissue pattern characterization systems are dominating in past studies [34–38, 43, 44, 54–57, 59, 60] but in recent studies gain the more attraction to design the computerized framework for breast



Benchmark dataset^a: (DDSM, MIAS) It is worth mentioning that the DDSM dataset contains images which are already labeled according to BIRADS density classes by the experts, however in case of MIAS dataset as well as in case of datasets collected by authors the images have been labeled according to BIRADS standard by the participating radiologists.

Fig. 2
Development of breast density classification system.

tissue pattern characterization using RBA based approach [39–42, 45–53, 58]. The study conducted by Kumar et al. [41] has developed a 4-class breast tissue pattern characterization system using GLCM-mean texture descriptors using RBA approach on 480 mammograms of DDSM dataset. This system yields the highest accuracy of 90.8% with the help of ENN classifier. The study done by Liu et al. [58] has attempted 4-class breast tissue pattern characterization on group of 88 mammograms which reports the highest accuracy of 86.4% using support vector machine classifier. It is worth to mention that only few studies has been conducted on Mammographic Image Analysis Society (MIAS) dataset using RBA approach. The highest achieved accuracy for MIAS dataset using RBA approach is 79.6% as reported in study [58].

Further, it can be visualized from Table 1, that most of the relevant work in past for 2-class breast tissue pattern characterization have been carried out on MIAS dataset using RBAs [45–53] and out of these studies the maximum accuracy of 97.2% have been reported in [47]. It is worth mentioning that 2-class breast tissue pattern characterization using DDSM dataset has been carried out using STBA [38]. It can be noticed that the highest prediction rate of 96.7% has been reported in Ref. [38] on 377 mammographic images of DDSM dataset using STBA. Few related studies have been carried out on limited number of mammographic images

collected by authors [56, 58]. The study reported in Ref. [58] has been carried out only on 88 mammographic images using RBA. However the study in Ref. [56] has been carried out on 132 mammographic images using STBA. The highest accuracy of 97.2% has been attended for 2-class breast tissue pattern characterization using ANN classifier on a collection of 144 mammograms [45].

It is worth observing that 91.2% the highest classification accuracy value has been reported in study [35] on DDSM dataset using RBA. Further it can also be noticed that 90.8% the maximum classification accuracy has been attained on DDSM dataset using RBA [41]. The present work can be directly compared to the work carried out on DDSM dataset using RBA approach.

Keeping in view the brief summary of the literature, the present work is different as it attempts to develop a computerized framework for breast tissue pattern characterization using RBA on DDSM dataset. It can be noted that RBA based approach for breast density classification is much simpler than the STBA, keeping in view that the STBA require automatic segmentation of breast tissue which involve additional steps, that is, background elimination and removal of pectoral muscle. These additional steps make STBAs more time consuming and complex. In RBA, the radiologist can easily mark square ROI at the heart of the breast where glandular tissues are prominently found in sufficient amount and the computer assisted framework shall predict the density class in real time clinical environment.

For breast density classification systems using RBA the accurate prediction of tissue pattern depends upon (a) location of ROI and (b) size of ROI. The extensive experiments carried out in study [61] indicate that the texture information of breast density is sufficient amount at the core region of the breast and concluded that the outcome of texture features for efficient description of breast tissue pattern information decreases as the location of fixed size ROI is varied from the long view center of breast region. Accordingly, in this study, different ROI sizes, that is, 32×32 , 64×64 , 128×128 , and 256×256 pixels have been manually extracted from heart location of the breast in order to obtain the optimal ROI size for efficient description of density information using various texture models.

The various texture features using (a) statistical texture feature models, that is, first order statistics (FOS), gray level co-occurrence matrix (GLCM), edge texture descriptors (EDGE), gray-level difference statistics (GLDS), neighborhood gray tone difference matrix (NGTDM), statistical feature matrix (SFM) and gray level run length matrix (GLRLM) based statistical models, (b) signal processing based texture feature models, that is, Laws' texture energy measures for kernel width 3, 5, 7, 9 and (c) transform domain texture feature models, that is, Fourier power spectrum (FPS), 2D discrete wavelet transform (DWT), 2D Gabor wavelet transform (GWT) are computed from each ROI and at the end application of proposed system is discussed using the ImageJ tool.

2 Materials and Methods

2.1 Description of Image Dataset

In this study 480 mediolateral oblique (MLO) view mammograms taken from a standard benchmark DDSM dataset have been used [62]. The DDSM dataset consists of a total of 2620 cases having four images of each case, that is, 2 MLO and 2 CLO views image. The description file of each case contains (a) 4-class BIRADS characterization done by the expert evaluation and (b) the coordinates of the lesion positions. The same set of images have been used for 2-class breast tissue pattern characterization by considering the (a) cases belonging to {BIRADS-I, BIRADS-II} classes in “fatty” class and (b) cases belonging to {BIRADS-III, BIRADS-IV} classes in “dense” class. Further, the bifurcation of this dataset into training and testing datasets is given in Fig. 3.

2.2 Optimization of ROI Size for Development of Computer Assisted Framework for Breast Tissue Pattern Characterization Using Digitized Screen Film Mammograms

In this study extensive experiments have been done for the selection of optimum size of ROI for the development of computer assisted frameworks for (a) 4-class breast tissue pattern characterization using digitized SFMs (Experiment 1), (b) 2-class (fatty, dense) breast tissue pattern characterization using digitized SFMs (Experiment 2).

The proposed ROI size optimization approach for the development of computer assisted framework for breast tissue pattern characterization using digitized SFMs is shown in Fig. 4.

The proposed ROI size optimization approach for the development of computer assisted framework for breast tissue pattern characterization using digitized SFMs consists of (a) ROI extraction phase (b) feature extraction phase, and (c) classification phase.

2.2.1 ROI extraction phase

The major facts observe by the participating radiologists that the textural appearances exhibited by different intensity value of the central region of breast are important for characterization into various tissue pattern classes. The same fact has been also experimentally confirmed in the work carried out by Li et al. [61]. Accordingly, in this work, ROIs of different size, that is, 32×32 , 64×64 , 128×128 , and 256×256 pixels have been manually extracted from the core heart location of the breast (behind the nipple) where glandular tissues are distributed in rich amounts from each mammogram. The sample images of BIRADS class mammograms with marked ROI are shown in Fig. 5.

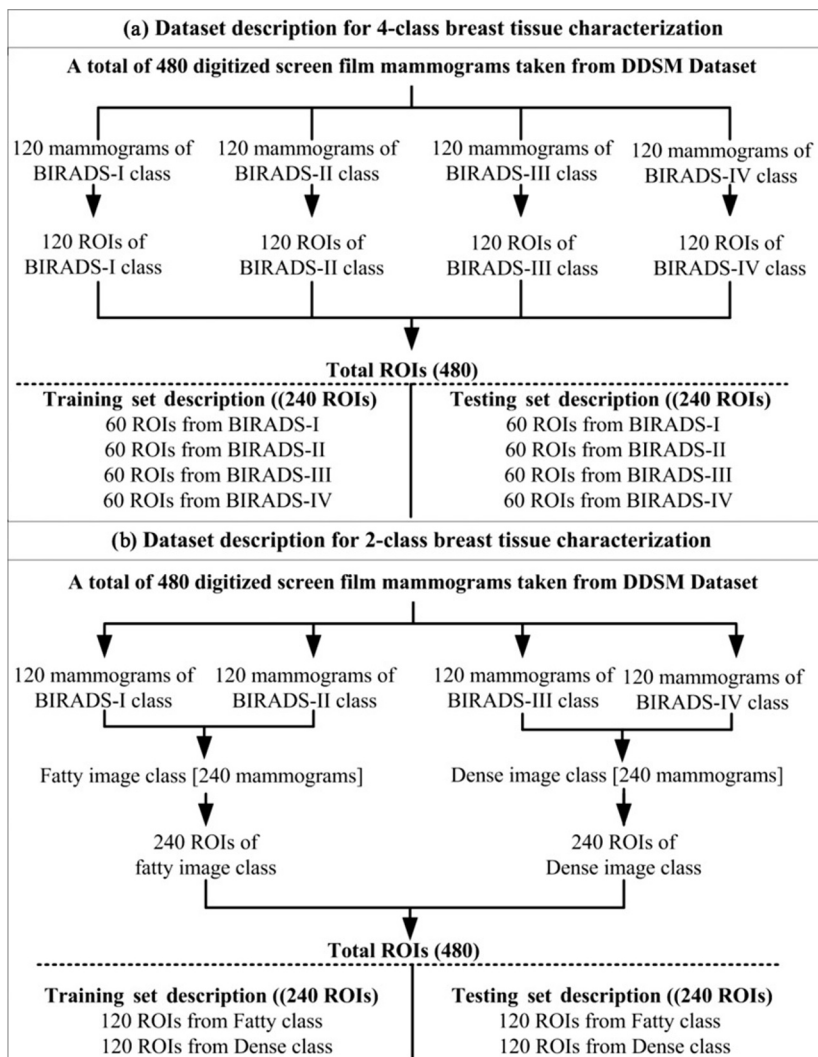
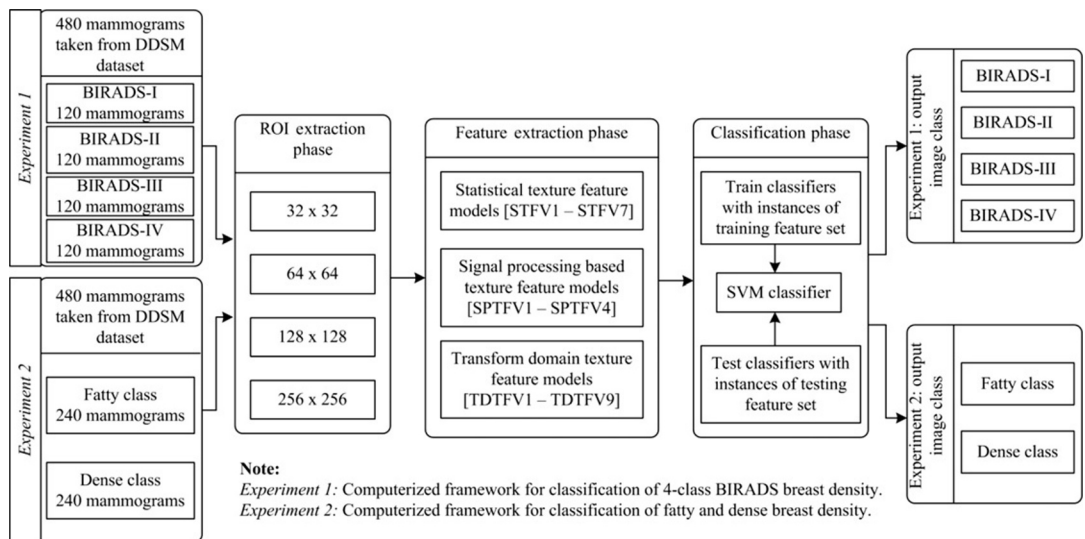


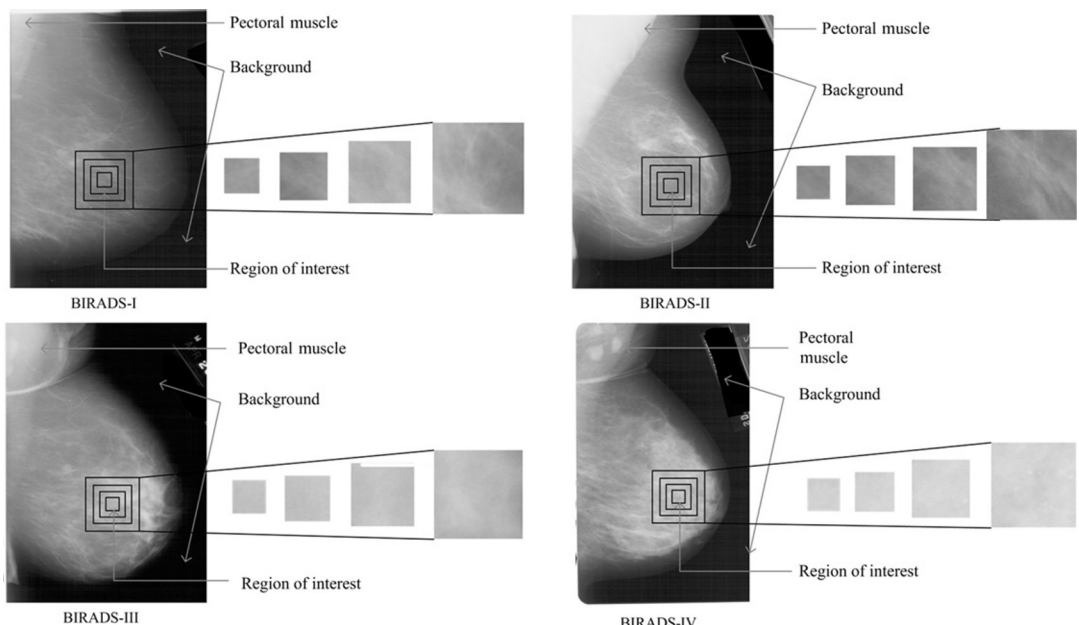
Fig. 3
Image dataset description.

2.2.2 Feature extraction phase

After the exhaustive literature review it has been found that the texture feature models, that is, statistical texture feature models, signal processing based texture feature models and transform domain texture feature models have been extensively used for classification of breast density [8, 23, 45–60]. Accordingly, in feature extraction phase, the texture feature vectors are computed for ROIs of size 32×32 , 64×64 , 128×128 , and 256×256 pixels using (a) statistical texture feature models (STFVs) (b) signal processing based texture feature models (SPTFVs), and (c) transform domain texture feature models (TDTFVs) and the

**Fig. 4**

Proposed ROI size optimization approach for the development of computer assisted framework for breast tissue pattern characterization using digitized screen film mammograms.

**Fig. 5**

Sample of BIRADS class mammograms with marked ROI.

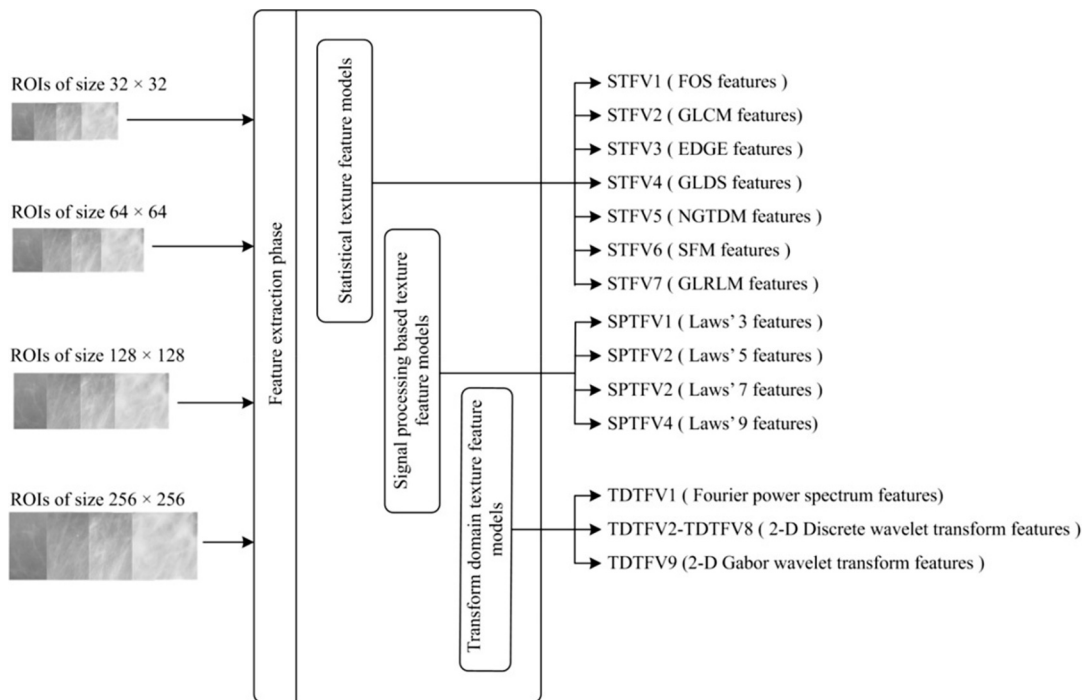


Fig. 6
Feature extraction phase.

performance of each feature set is analyzed for each ROI size. The block diagram of feature extraction phase is shown in Fig. 6.

The brief description of various texture feature models used in the present work is given here.

2.2.2.1 Statistical texture feature models

The statistical texture feature models [23, 46, 51, 63–75] are associated with spatial distribution of intensities levels of various pixels in an image. These texture feature models are further categorized as first order statistical model, second order statistical model and higher order statistical models. The brief description of different statistical texture feature vectors (STFVs) extracted using statistical texture feature models used in this study are reported in Fig. 7.

2.2.2.2 Signal processing based texture feature models

The signal processing based texture feature vectors (SPTFVs) extracted in the present work are computed using Laws' mask texture energy analysis.

Laws' mask analysis In this work, the Laws' descriptors [50, 76] have been computed using Laws' 3, Laws' 5, Laws' 7, and Laws' 9. If the Laws' energy descriptors are computed using 1D filters of kernel width 3, a total of nine Laws' masks (2D filters) are obtained by

TFM	TFV	Extracted features	l
FOS	STFV1	Average gray level, standard deviation, smoothness, third moment, uniformity, entropy	6
GLCM	STFV2	Angular second moment, contrast _{GLCM} , correlation, variance, inverse difference moment, sum average, sum variance, sum entropy, entropy _{GLCM} , difference variance, difference entropy, information measures of correlation-1, information measures of correlation-2	13
EDGE	STFV3	Absolute gradient mean, absolute gradient variance	2
GLDS	STFV4	contrast _{GLDS} , homogeneity, energy, entropy, mean	5
NGTDM	STFV5	contrast _{NGTDM} , coarseness _{NGTDM} , periodicity, roughness	4
SFM	STFV6	homogeneity, contrast _{SFM} , energy, entropy _{NGTDM}	4
GLRLM	STFV7	short run emphasis, short run low gray level emphasis, short run high gray level emphasis, long run emphasis, long run low gray level emphasis, long run high gray level emphasis, gray level non uniformity, run length non uniformity, high gray level run emphasis, low gray level run emphasis, run percentage	11

Note: *TFM*, texture feature model; *TFV*, texture feature vector; l , length of TFV.

Fig. 7
Different TFVs extracted using statistical texture feature models.

combining these 1D filters in a combinatorial manner. The obtained 2D masks are normalized and then pass it through the texture energy measurement filter resulting in texture energy measurement images (TEM). Out of these nine (TEM) 2D Laws' masks, three masks are identical to the other three, if they are rotated by 90°. By combining the pairs of identical masks, six rotation invariant images (TRs) are obtained for each ROI. From the TR images compute the desired statistical features, that is, mean standard deviation, entropy, skewness, and kurtosis. Thus for kernel width 3, 30 statistics are obtained from 6 TRs. The Laws' texture features measurement steps with example of Laws' 3 is given in Fig. 8.

The brief description of different TFVs extracted using signal processing based texture feature models used in this work is reported in Fig. 9.

2.2.2.3 Transform domain texture feature models

From the studies in literature, it can be observed that texture description in transform domain has been carried out [48, 77, 78] using various multiresolution schemes such as Fourier power spectrum (FPS), 2D DWT and 2D GWT. The brief description of various transform domain texture feature models used in the present work is given here.

Fourier power spectrum based texture feature model: The TDTFV1 (as shown in first row of Table 2, computed using Fourier power spectrum based texture feature model) consists of spectral features, that is, radial sum and angular sum [79].

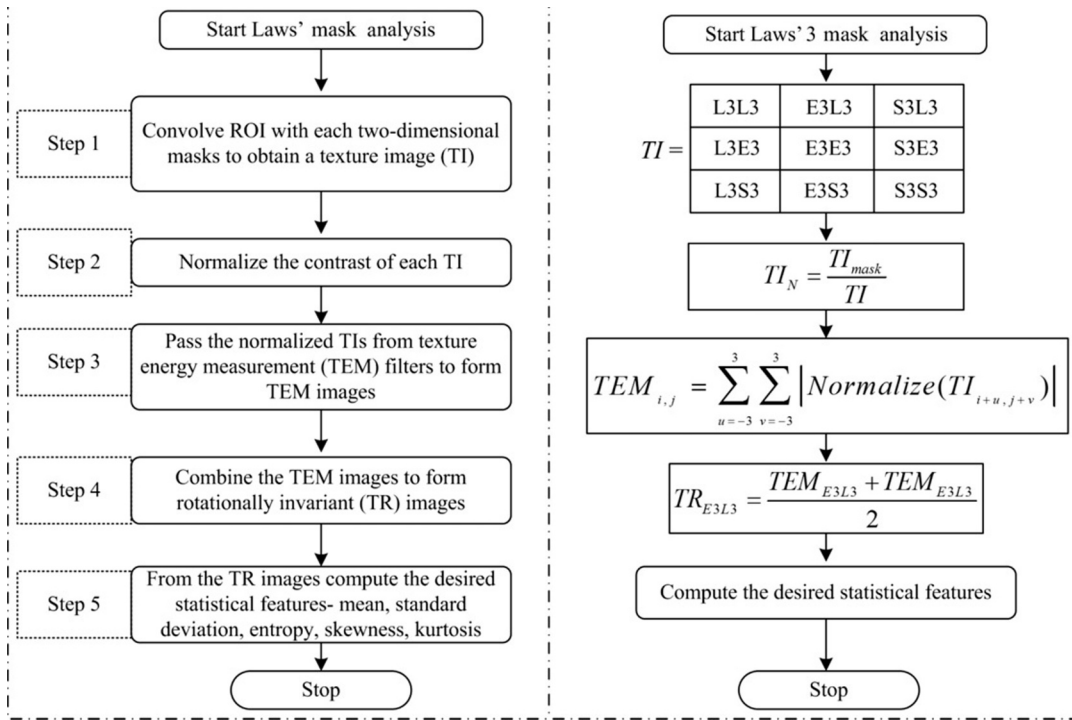


Fig. 8
Laws' texture features measurement steps with example of Laws' 3.

TFM	TFV	Length of 1D filter	TFM	No. of 2D Laws' masks (A)	TRs obtained from identical filter pairs (B)	Total TRs (A - B)	I
Laws' 3	SPTFV1	3	L3=[1, 2, 1] E3=[-1, 0, 1] S3=[-1, 2, -1]	9	3	6	30
Laws' 5	SPTFV2	5	L5=[1, 4, 6, 4, 1] E5=[-1, 2, 0, 2, 1] S5=[-1, 0, 2, 0, -1] W5=[-1, 2, 0, -2, 1] R5=[1, -4, 6, -4, 1]	25	10	15	75
Laws' 7	SPTFV3	7	L7=[1, 6, 15, 20, 15, 6, 1] E7=[-1, -4, -5, 0, 5, 4, 1] S7=[-1, -2, 1, 4, 1, -2, -1]	9	3	6	30
Laws' 9	SPTFV4	9	L9=[1, 8, 28, 56, 70, 56, 28, 8, 1] E9=[1, 4, 4, -4, -10, -4, 4, 4, 1] S9=[1, 0, -4, 0, 6, 0, -4, 0, 1] W9=[1, -4, 4, -4, -10, 4, 4, -4, 1] R9=[1, -8, 28, -56, 70, -56, 28, -8, 1]	25	10	15	75

Note: *TFM*, texture feature model; *TFV*, texture feature vector; *SPTFV*, signal processing based texture feature vector; *TRs*, rotational invariant texture images; *I*, length of TFV i.e. 5 statistics \times no. of TR images.

Fig. 9
Different TFVs extracted using signal based texture feature models.

Table 2 Different TTVs extracted using transform domain texture feature models

TFM	TFV	Extracted Features	I
FPS	TDTFV1	Radial sum, angular sum	2
2D DWT	TDTFV2	$\frac{\ A_2\ _F^2}{\text{area}(A_2)}, \frac{\ D_2^{(h)}\ _F^2}{\text{area}(D_2^{(h)})}, \frac{\ D_2^{(v)}\ _F^2}{\text{area}(D_2^{(v)})}, \frac{\ D_2^{(d)}\ _F^2}{\text{area}(D_2^{(d)})}, \frac{\ D_1^{(h)}\ _F^2}{\text{area}(D_1^{(h)})}, \frac{\ D_1^{(v)}\ _F^2}{\text{area}(D_1^{(v)})}, \frac{\ D_1^{(d)}\ _F^2}{\text{area}(D_1^{(d)})}$	7
	TDTFV3	$\frac{\ D_1^{(h)}\ _F^2}{\text{area}(D_1^{(h)})}, \frac{\ D_1^{(v)}\ _F^2}{\text{area}(D_1^{(v)})}, \frac{\ D_1^{(d)}\ _F^2}{\text{area}(D_1^{(d)})}$	3
	TDTFV4	$\frac{\ D_1^{(h)}\ _F^2}{\text{area}(D_1^{(h)})}, \frac{\ D_1^{(v)}\ _F^2}{\text{area}(D_1^{(v)})}, \frac{\ D_1^{(d)}\ _F^2}{\text{area}(D_1^{(d)})}, \frac{\ D_2^{(h)}\ _F^2}{\text{area}(D_2^{(h)})}, \frac{\ D_2^{(v)}\ _F^2}{\text{area}(D_2^{(v)})}, \frac{\ D_2^{(d)}\ _F^2}{\text{area}(D_2^{(d)})}$	6
	TDTFV5	$\frac{\ D_1^{(h)}\ _F^2}{\text{area}(D_1^{(h)})}, \frac{\ D_1^{(v)}\ _F^2}{\text{area}(D_1^{(v)})}, \frac{\ D_1^{(d)}\ _F^2}{\text{area}(D_1^{(d)})}, \frac{\ D_2^{(d)}\ _F^2}{\text{area}(D_2^{(d)})}$	4
	TDTFV6	$\frac{\ A_2\ _F^2}{\text{area}(A_2)}, \frac{\ D_1^{(h)}\ _F^2}{\text{area}(D_1^{(h)})}, \frac{\ D_1^{(v)}\ _F^2}{\text{area}(D_1^{(v)})}, \frac{\ D_1^{(d)}\ _F^2}{\text{area}(D_1^{(d)})}$	4
	TDTFV7	$\frac{\ A_2\ _F^2}{\text{area}(A_2)}, \frac{\ D_2^{(h)}\ _F^2}{\text{area}(D_2^{(h)})}, \frac{\ D_2^{(v)}\ _F^2}{\text{area}(D_2^{(v)})}, \frac{\ D_2^{(d)}\ _F^2}{\text{area}(D_2^{(d)})}$	4
	TDTFV8	$\frac{\ D_2^{(h)}\ _F^2}{\text{area}(D_2^{(h)})}, \frac{\ D_2^{(v)}\ _F^2}{\text{area}(D_2^{(v)})}, \frac{\ D_2^{(d)}\ _F^2}{\text{area}(D_2^{(d)})}$	3
2D GWT	TDTFV9	Mean and standard deviation are calculated for seven orientation $22.5^\circ, 45^\circ, 67.5^\circ, 90^\circ, 112.5^\circ, 135^\circ, 157.5^\circ$ and three magnitude values 0, 1, and 2 ($3 \times 7 \times 2 = 42$)	42

Note: *TFM*, texture feature model; *TDTFV*, transform domain texture feature vector; *I*, length of TTV; *A*, approximate subband image; *D*, detail subband image; *h*, horizontal; *v*, vertical; *d*, diagonal; *A_i* or *D_i*, *i* represent *i*th level of decomposition; *area*, total number of pixels to the respective subband image.

2D discrete wavelet transform based texture feature model: In the present work each ROI image has been decomposed up to second level by using 2D DWT multiresolution scheme with different compact supporting filters. After the exhaustive experiments it has been found that the compact support filter “haar” yields the maximum discrimination information between different density patterns. Thus “haar” wavelet filter is considered for this study. After decomposition seven subband images, that is, one approximate subband image and six orientation selective detail subband images are generated for each ROI image as shown in Fig. 10. Normalized energy values are computed from each of these subband images.

The brief description of different TFVs (TDTFV2 to TDTFV8) extracted using 2D discrete wavelet transform based texture feature model is reported in Table 2.

2D Gabor wavelet transform based texture feature model: In the present work, 2D GWT based texture descriptor have been computed using three magnitude values 0, 1, and 2 and seven orientation values 22.5° , 45° , 67.5° , 90° , 112.5° , 135° , and 157.5° . This gives a resulting in a group of 21 (7×3) wavelets of Gabor filter bank. It is worth mentioning that these 21 wavelets capture energy at a particular magnitude value and orientation value. The real parts of Gabor filter bank is shown in Fig. 11.

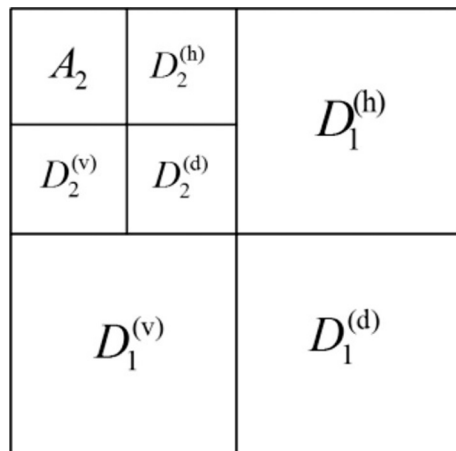
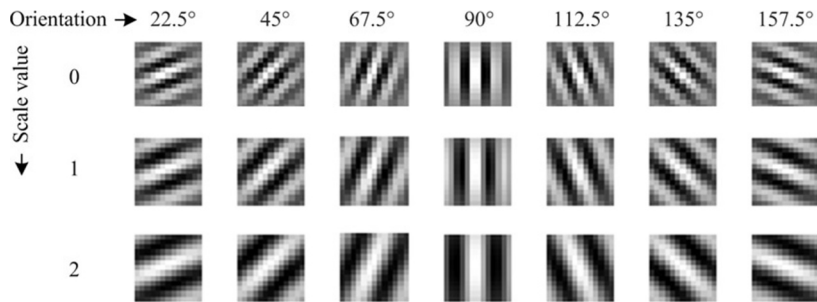


Fig. 10

2D DWT tree up to second level decomposition. Note: A_2 , approximate subband feature image at second level of decomposition; $D_2^{(h)}$, detail coefficient of horizontal subband feature image at second level of decomposition; $D_2^{(d)}$, detail coefficient of diagonal subband feature image at second level of decomposition; $D_2^{(v)}$, detail coefficient of vertical subband feature image at second level of decomposition; $D_1^{(h)}$, detail coefficient of horizontal subband feature image at second level of decomposition; $D_1^{(d)}$, detail coefficient of diagonal subband feature image at first level of decomposition; $D_1^{(v)}$, detail coefficient of vertical subband feature image at first level of decomposition; A_i or D_i , i th level of decomposition.

**Fig. 11**

Real parts of Gabor filter bank for seven orientations and three magnitude values.

The group of 21 Gabor filter bank is convolved with an input ROI image to getting filtered images called features images. Each feature image depicts the texture information at a certain magnitude and orientation. Computing mean and standard deviation statistics from these 21 Gabor outputs or feature images results in a feature vector of length 42 (i.e., 2 statistics for 21 feature images). The brief description of different TFV (i.e., TDTFV9) extracted using 2D Gabor wavelet transform based texture feature models used in this work is reported in [Table 2](#).

2.3 Classification Phase

To deploy the proposed work two different classification modules have been invoked using support vector machine (SVM) classifier.

2.3.1 4-Class breast tissue pattern characterization module

This classification module uses one-against-one (OAO) approach (available in LibSVM library [[80](#)]) by constructing $X(X - 1)/2$ binary classifiers (here, X is the number of classes).

It is necessary to train each binary classifier separately for the differentiation between a pair of classes, and majority voting technique is used for the making prediction of an input test ROI. In 4-class breast density classification, the prediction of the class of the test ROI is made by majority voting mechanism on the predictions of six binary classifiers, that is, SVM (BIRADS-I vs BIRADS-II), SVM (BIRADS-I vs BIRADS-III), SVM (BIRADS-I vs BIRADS-IV), SVM (BIRADS-II vs BIRADS-III), SVM (BIRADS-II vs BIRADS-IV), and SVM (BIRADS-III vs BIRADS-IV).

2.3.2 2-Class breast tissue pattern characterization module

It has been implemented using binary SVM approach available in LibSVM library [[80](#)].

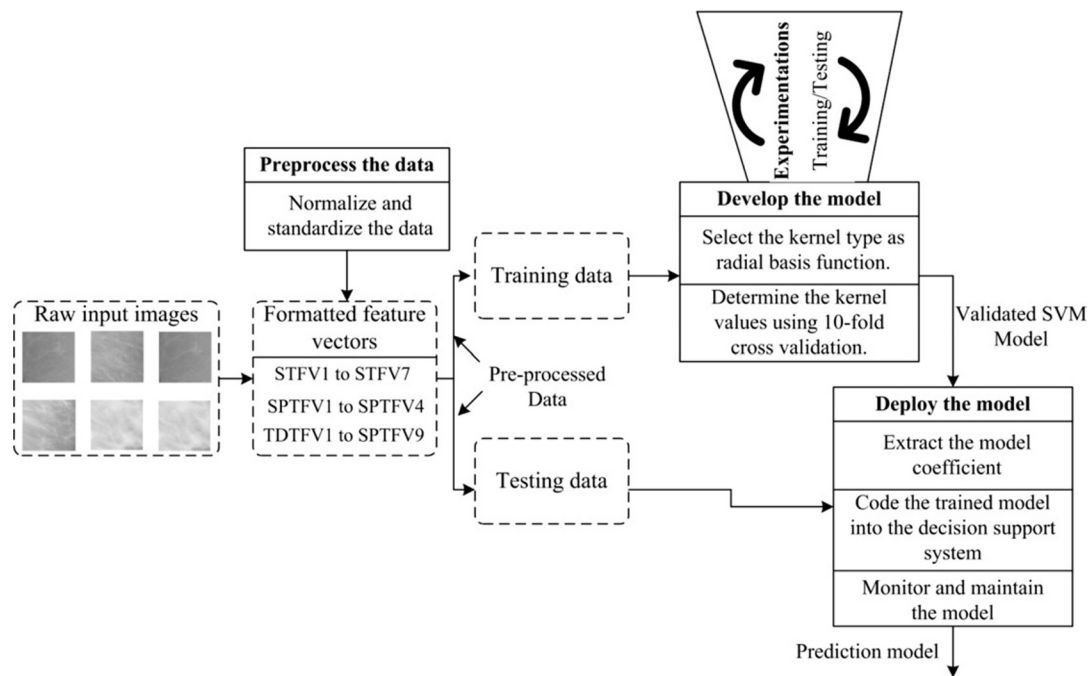


Fig. 12
Development of SVM model.

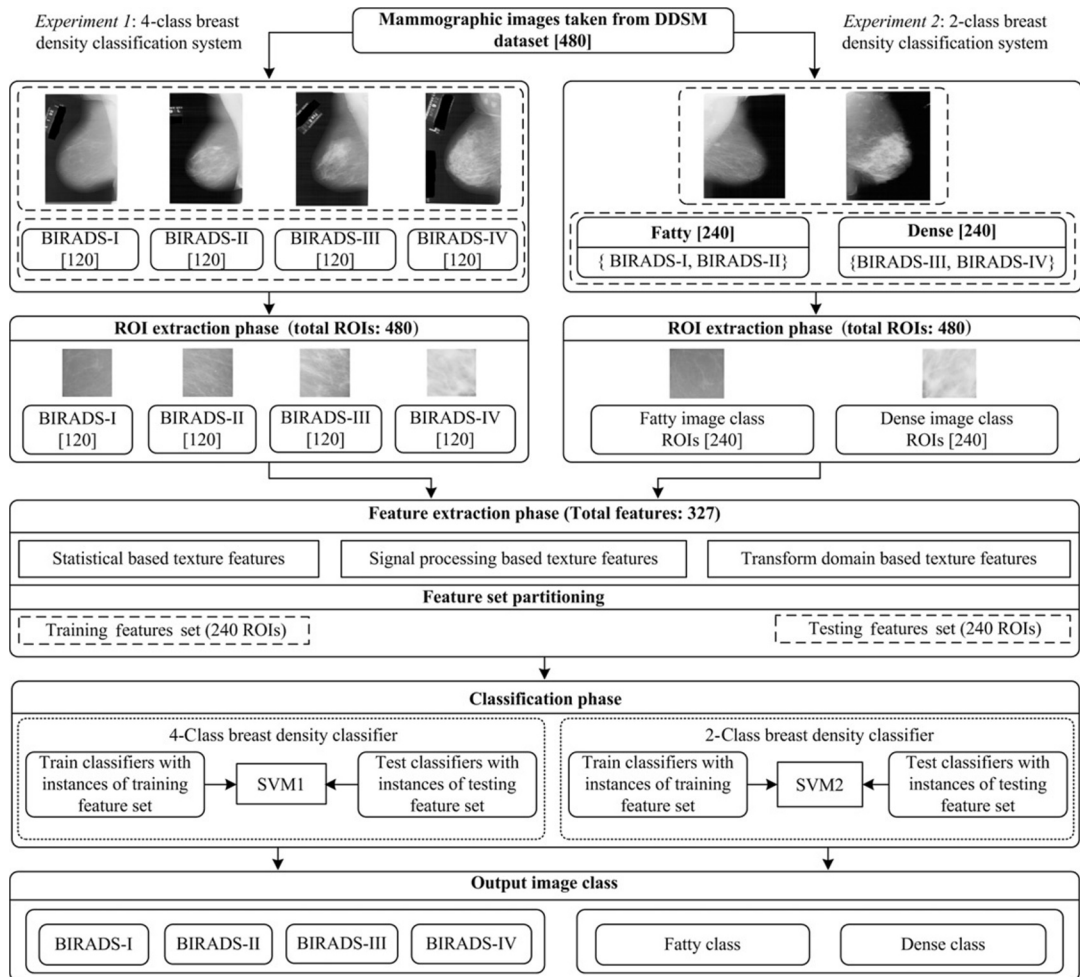
2.3.3 SVM classifier

In the present work, RBF kernel function based support vector machine classifier is imported from LibSVM library. The development of SVM model is shown in Fig. 12. For obtaining the optimal values of regularization parameter C , and soft marginal kernel parameter γ for Gaussian RBF kernel, a grid search procedure has been applied, by conducting 10-fold cross validation training accuracy for each combination of (C, γ) , such that, $C \in \{2^{-4}, 2^{-3}, \dots, 2^{15}\}$ and $\gamma \in \{2^{-12}, 2^{-11}, \dots, 2^4\}$.

3 Experiments and Results

In this study, various examinations have been carried out on ROIs of different size, that is, 32×32 , 64×64 , 128×128 , and 256×256 pixels for breast density classifications. These ROIs are fed to feature extraction phase. In feature extraction phase various texture features are computed, that is, statistical texture feature vectors (STFV1-STFV7), signal processing based texture feature vectors (SPTFV1-SPTFV4) and transform domain texture feature vectors (TDTFV1-TDTFV9). These texture feature vectors (TFVs) are fed to SVM classifier in classification phase.

The pictorial representation of work flow diagram for selection of optimum ROI size for the development of computer assisted framework for breast tissue pattern characterization using digitized SFMs is given in Fig. 13.

**Fig. 13**

Experimental work flow diagram for the selection of optimum ROI size for the development of computer assisted framework for breast tissue pattern characterization using digitized SFMs.

3.1 Experiment 1: Experiment Carried Out for the Selection of Optimum ROI Size for the Development of Computer Assisted Framework for 4-Class Breast Tissue Pattern Characterization Using Digitized SFMs

In this experiment the performance of various TFVs has been computed for 4-class breast tissue pattern characterization task using SVM1 classifier. The achieved performance of this experiment is given in [Table 3](#).

From [Table 3](#), it can be observed that for all the 20 TFVs (7 STFVs +4 SPTFVs +9 TDTFVs) the highest characterization accuracy is achieved for 128×128 pixels ROIs size (bolded in the [Table 3](#)). It can also be noticed that the maximum accuracy of 79.5% has been gained by STFV2

Table 3 Achieved performance of various TTVs for 4-class breast tissue pattern characterization using SVM1 classifier

TTVs	(l)	Accuracy (%)			
		32 × 32	64 × 64	128 × 128	256 × 256
Classification performance of statistical texture feature vectors (STFV1-STFV7) for different ROI sizes					
STFV1	6	49.5	57.9	69.1	68.7
STFV2	13	47.5	56.6	79.5	66.6
STFV3	2	46.2	45.8	48.7	45.0
STFV4	5	33.7	38.7	47.1	46.6
STFV5	5	45.0	43.7	66.6	61.2
STFV6	4	43.7	47.0	51.6	47.0
STFV7	11	49.1	55.0	66.6	61.6
Classification performance of signal processing based texture feature vectors (SPTFV1-SPTFV4) for different ROI sizes					
SPTFV1	30	50.0	51.6	64.1	56.2
SPTFV2	75	50.8	49.5	73.3	70.0
SPTFV3	30	51.6	55.8	66.2	66.2
SPTFV4	75	43.3	54.5	69.5	63.3
Classification performance of transform domain texture feature vectors (TDTFV1-TDTFV9) for different ROI sizes					
TDTFV1	2	50.4	57.5	60.4	60.0
TDTFV2	7	46.2	56.2	64.7	64.5
TDTFV3	3	40.0	47.5	48.3	45.8
TDTFV4	6	36.6	47.5	50.8	49.1
TDTFV5	4	30.0	50.4	49.1	49.1
TDTFV6	5	44.5	51.2	57.0	56.2
TDTFV7	4	48.3	55.0	62.0	53.7
TDTFV8	3	35.8	46.25	50.8	50.4
TDTFV9	42	46.6	49.1	65.0	60.8

Note: TTVs, texture feature vectors; l, length of TTV; STFV, statistical texture feature vector; SPTFV, signal processing based texture feature vector; TDTFV, transform domain texture feature vector.

(i.e., GLCM texture descriptor at “d” = 10, where d represent interpixel distance). The classification performance yielded by STFV2 is given in [Table 4](#) and pictorial representation for the performance of STFV2 is shown in [Fig. 14](#).

From [Table 4](#), it can be noticed that STFV2 (i.e., GLCM texture descriptor at “d” = 10) yields the highest OCA value 79.5% with ICA values of 90.0%, 80.0%, 51.6%, and 96.6% for B-I, B-II, B-III, and B-IV class.

The results of the experiment demonstrate that the ROI size of 128 × 128 pixels extracted from the core region of the breast provides sufficient information for differentiation in various breast tissue pattern classes.

Table 4 Classification performance yielded by STFV2 for 4-class breast tissue pattern classification

TFV (l)		CM				Accuracy (%)	
		B-I	B-II	B-III	B-IV	ICA	OCA
STFV2 (13)	B-I	54	4	2	0	90.0	79.5
	B-II	5	48	5	2	80.0	
	B-III	0	14	31	15	51.6	
	B-IV	0	0	2	58	96.6	

Note: TFV , texture feature vector; $STFV$, statistical texture feature vector; l , length of TFV; CM , confusion matrix; $B-I$, BIRADS-I; $B-II$, BIRADS-II; $B-III$, BIRADS-III; $B-IV$, BIRADS-IV; OCA , overall classification accuracy; ICA , individual class accuracy.

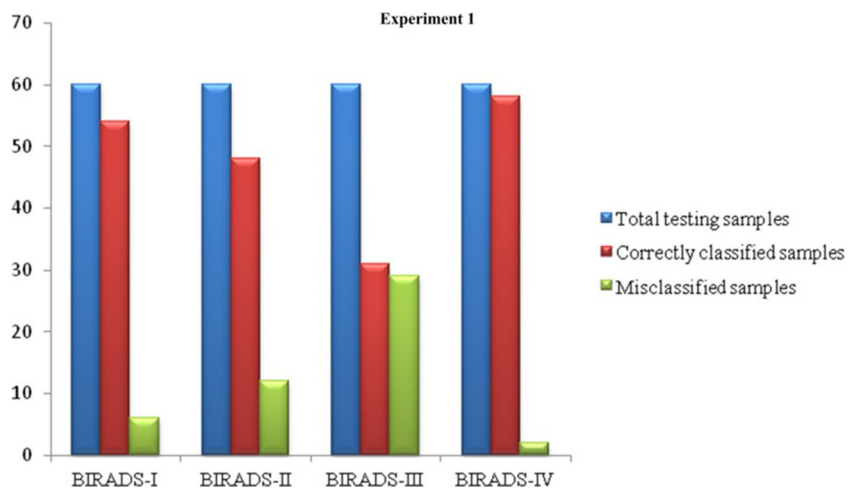


Fig. 14
Representation of performance for Experiment 1 using STFV2.

3.2 Experiment 2: Experiment Carried Out for the Selection of Optimum ROI Size for the Development of Computer Assisted Framework for 4-Class Breast Tissue Pattern Characterization Using Digitized SFMs

In this experiment the performance of various TFVs has been computed for 2-class breast tissue pattern classification task using SVM2 classifier. The achieved performance of this experiment is given in [Table 5](#).

From [Table 5](#), it can be observed that for all the 20 TFVs (7 STFVs +4 SPTFVs +9 TDTFVs) the highest prediction rate value is obtained for 128×128 pixels of ROIs size (bolded in the [Table 5](#)). It can also be noticed that the maximum accuracy of 91.2% is yielded by SPTFV1 (i.e., texture features computed using Laws' masks of kernel width 3).

Table 5 Classification performance of various TFVs for 2-class breast tissue pattern characterization using SVM2 classifier

TFVs	(I)	Accuracy (%)			
		32 × 32	64 × 64	128 × 128	256 × 256
Classification performance of statistical texture feature vectors (STFV1-STFV7) for different ROI sizes					
STFV1	6	81.6	82.0	89.1	89.1
STFV2	13	77.5	81.2	88.7	88.5
STFV3	2	81.6	85.0	85.8	77.0
STFV4	5	57.0	65.0	66.6	66.2
STFV5	5	77.5	77.9	83.3	82.5
STFV6	4	64.5	62.9	72.0	65.6
STFV7	11	76.2	80.0	87.9	87.9
Classification performance of signal processing based texture feature vectors (SPTFV1-SPTFV4) for different ROI sizes					
SPTFV1	30	81.2	80.8	91.2	82.0
SPTFV2	75	80.8	81.7	89.5	87.9
SPTFV3	30	82.0	84.5	89.5	87.5
SPTFV4	75	78.3	82.9	87.5	87.5
Classification performance of transform domain texture feature vectors (TDTFV1-TDTFV9) for different ROI sizes					
TDTFV1	2	78.7	83.7	86.3	85.0
TDTFV2	7	80.8	79.1	88.3	87.0
TDTFV3	3	66.2	70.0	72.9	72.5
TDTFV4	6	62.0	66.2	72.9	71.2
TDTFV5	4	63.7	65.8	72.0	71.2
TDTFV6	5	80.8	80.4	87.0	86.2
TDTFV7	4	80.0	81.6	88.3	85.8
TDTFV8	3	67.5	69.5	83.3	70.0
TDTFV9	42	80.0	81.6	87.0	86.6

Note: *STFV*, statistical texture feature vector; *SPTFV*, signal processing based texture feature vector; *TDTFV*, transform domain texture feature vector.

Table 6 Classification performance yielded by SPTFV1 for 2-class breast density characterization

TFV (I)	CM		Accuracy (%)	
	F	D	ICA	OCA
SPTFV1 (30)	F	112	8	93.3
	D	13	107	89.1

Note: *SPTFV*, signal processing based texture feature vector; *F*, fatty image class; *D*, dense image class; *CM*, confusion matrix.

The classification performance yielded by SPTFV1 for 2-class breast density classes is reported in [Table 6](#) and pictorial representation for the performance of SPTFV1 is shown in [Fig. 15](#).

From [Table 6](#), it can be noticed that SPTFV1 (i.e., Laws' masks of kernel width 3 features) yields the maximum OCA value of 91.2% with ICA values of 93.3% and 89.1% for fatty class and dense image class.

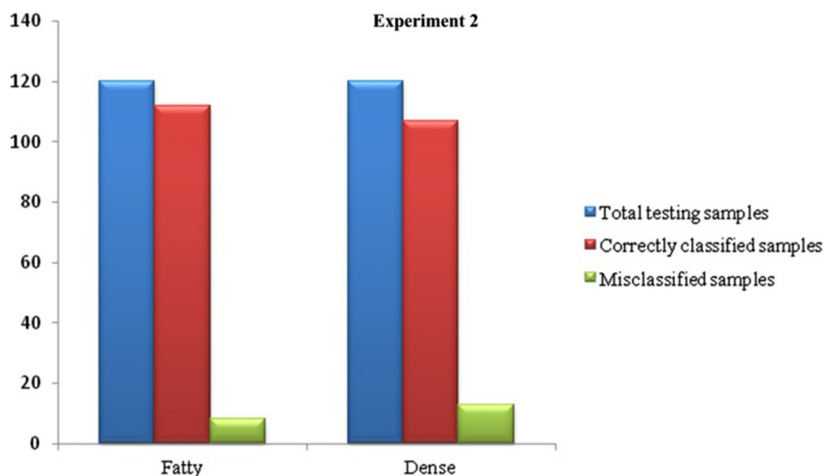


Fig. 15
Representation of performance for Experiment 2 using SPTFV1.

The result obtained from the exhaustive experiment demonstrate that the ROI size of 128×128 pixels manually extracted from the core region of the breast provides sufficient information for differentiation in various breast tissue pattern classes.

3.3 Statistical Analysis

The statistical analysis of the proposed system is performed by using Cohen's kappa coefficient [81].

(a) For 4-class breast tissue pattern characterization

Observed accuracy (po) = 0.7958	Expected accuracy (pe) = 0.2500
$po-pe = 0.5458$	$1-pe = 0.7500$
Cohen's kappa value = 0.7278	kappa error = 0.0347

The Cohen's kappa value for the computerized framework for 4-class breast tissue pattern characterization is 0.7278. The obtained kappa value shows that the proposed system has considerable importance for the radiologists to classify between different BIRADS breast density classes.

(b) For 2-class breast density characterization

Observed accuracy (po) = 0.9125	Expected accuracy (pe) = 0.5000
$po-pe = 0.4125$	$1-pe = 0.5000$
Cohen's kappa value = 0.8250	kappa error = 0.0365

The Cohen's kappa value for the computerized framework for 2-class breast density is 0.825. The obtained kappa value shows that the proposed system is acceptable and suitable for the radiologists to classify between fatty and dense breast density classes.

3.4 Comparative Analysis

The comparative analysis of different experiments performed for the present work for breast tissue pattern characterization is reported in [Table 7](#). The comparative study is analyzed in terms of misclassified instances and performance of 4-class breast tissue pattern characterization and 2-class breast tissue pattern characterization system.

From the [Table 7](#), it is observed that the designed classification framework by *experiment 2* is better than the proposed classification framework by *experiment 1* with respect to the number of TMIs, OCA value as well as kappa value. Out of 240 testing instances only 21 instances are misclassified at *experiment 2* while 49 instances are misclassified at *experiment 1*. It can also be noticed that the obtained OCA value for *experiment 1* is 79.5% and 91.2% for experiment 2. The Cohen's kappa value of experiment 2 is 0.8250 while 0.7278 is for *experiment 1*, which shows the classification framework designed using *experiment 2* is more reliable and suitable for the real time breast density classification problem.

The present work can be directly compared to the work carried out on DDSM dataset using RBA approach. For 4-class and 2-class problem, it is directly compared with study carried out by Kumar et al. [41] and Kumar et al. [42], respectively. The outcome of the comparison is summarized in [Fig. 16](#).

3.5 Application of the Proposed Work

In routine clinical practice, the participating radiologist finds large number of cases of dense mammograms in which lesions cannot be visible by looking at the raw image, that is, if the lesions are behind the glandular ducts. For an input image if the prediction of proposed

Table 7 Comparative analysis of various experiments carried out in this study for breast density classification

Considered		Class	No. of TIs	No. of MIs	ICA (%)	TMIs	OCA (%)	Kappa Value
Experiment 1	B-I	60	6	90.0	49	79.5	0.7278	
	B-II	60	12	80.0				
	B-III	60	29	51.6				
	B-IV	60	2	96.6				
Experiment 2	Fatty	120	8	93.3	21	91.2	0.8250	
	Dense	120	13	89.1				

Note: *TIs*, testing instances; *MIs*, misclassified instances; *TMIs*, total misclassified instances; *OCA*, overall classification accuracy. (21 testing instances are misclassified by experiment 2.)

Comparison between earlier study carried out by Kumar et al. [41, 42] and proposed work for 4-class and 2-class breast tissue density characterization using RBA				
Author(s), Year	No. of Images	Classifier Used	Individual Class Accuracy (%)	
Kumar et al. [41]	480	Ensemble of neural networks	B1	98.3
			B2	91.6
			B3	80.0
			B4	93.3
Proposed	480	Support vector machine (SVM)	B1	90.0
			B2	80.0
			B3	51.6
			B4	96.6
Comparison between earlier study carried out by Sharma, et al. 2015 and proposed work for 2-class breast tissue density characterization using RBA				
Author(s), Year	No. of Images	Classifier Used	Individual Class Accuracy (%)	
Kumar, et al. [42]	480 (from DDSM)	Support vector machine (SVM)	Fatty	98.3
			dense	89.1
Proposed	480 (from DDSM)	Support vector machine (SVM)	Fatty	93.3
			dense	89.1

Fig. 16

Comparison between earlier studies carried out by Kumar et al. [41, 42] and proposed work.

classification framework is dense and lesions are not clearly visible then for such type of cases participating radiologist can enhance the mammograms by varying the contrast and brightness using the ImageJ processing tool [82, 83] to detect masked lesions.

In case of B-I and B-II density classes the lesions are easily visible without the need of any processing. The samples of these cases taken from DDSM dataset are given in Fig. 17.

In case of dense mammograms if lesions are behind the glandular ducts then they are clearly visible without any processing. Fig. 18 depicts the dense mammograms from the DDSM dataset in which lesions are clearly visible.

In case of dense image class (B-III and B-IV) the lesions are masked behind the glandular tissue shown in the labeled image can be detected only after processing. The sample of these cases taken from DDSM dataset is shown in Fig. 19.

For the application of proposed characterization framework radiologists used for breast tissue pattern classification and radiologists use the ImageJ software to preprocess dense mammograms in order to detect the lesions. Indeed, the accuracy of the proposed system is sensitive to the accuracy of the radiologists.

In future an automatic method for evaluation of dense mammograms shall be developed using the same set of texture models so that the masked lesions behind the glandular ducts are visible after double screening.

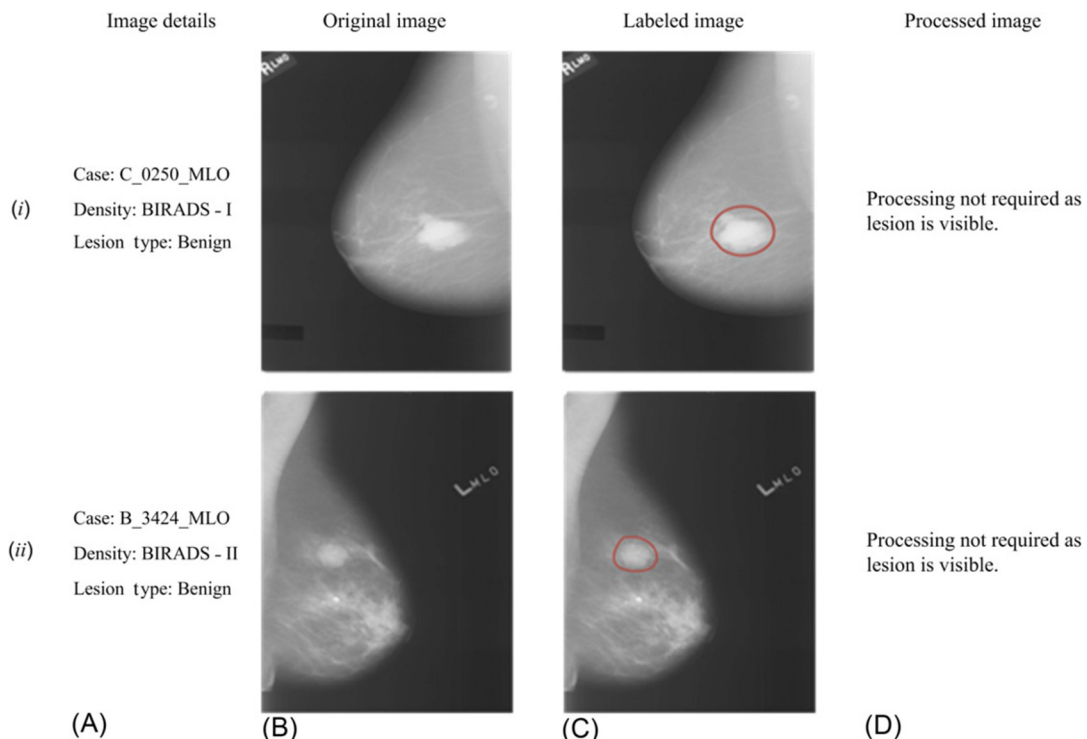


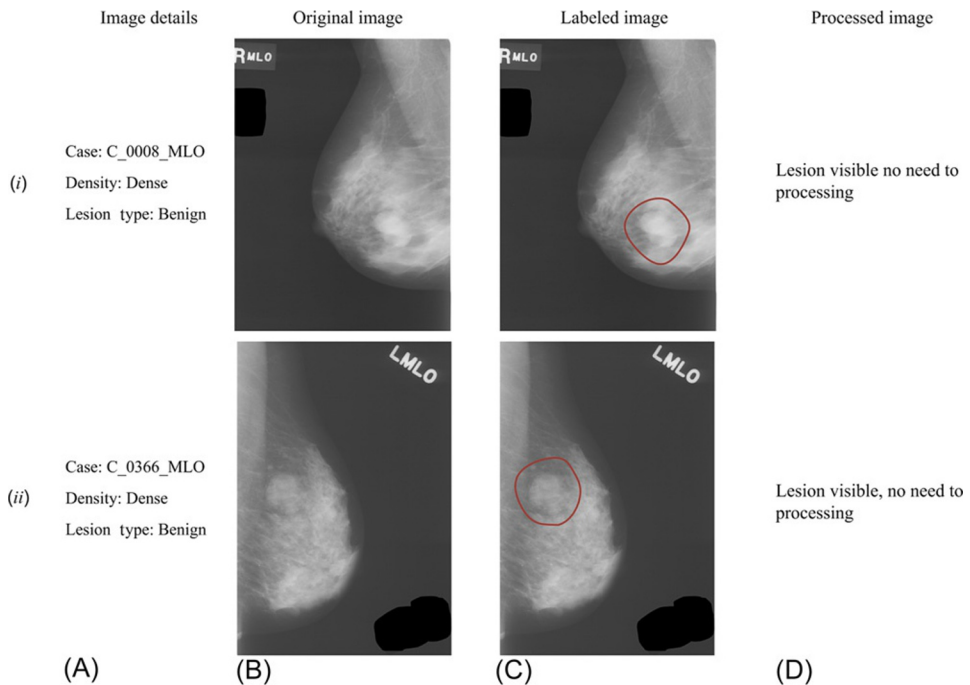
Fig. 17

Sample images of fatty, that is, images belongs to BIRADS-I, BIRADS-II. (A) Image details, (B) original image, (C) labeled image with lesion marked, and (D) processed image.

Further for an unknown test ROI, if the prediction of 2-class breast density characterization module is “dense” and the lesion is around the glandular ducts then the radiologist should double screen the mammograms or enhance the mammograms by varying the brightness and contrast with the help of ImageJ software detection of masked lesions in dense mammogram as shown in Fig. 20.

In daily routine clinical environment, during screening mammography the radiologist finds large number of cases of dense mammograms in which lesions cannot be detected by looking at the raw image. Therefore, accurate prediction of breast tissue pattern class is essential so that the radiologist can double screen these dense mammograms for detection of masked lesions, if any.

The outcomes of the study show that the ROI size of 128×128 pixels manually extracted from the core region of the breast provide significant information to discrimination between various breast tissue pattern classes. It may be also noticed that higher accuracy of 91.2% is achieved by 2-class breast density classification module in comparison to 79.5% as achieved by 4-class breast tissue pattern characterization framework. Therefore, the present

**Fig. 18**

Sample images of dense image class where lesion is visible. (A) Image details, (B) original image, (C) labeled image with lesion marked, and (D) processed image. Note: Lesion is not behind the glandular ducts and it is visible, so processing not required.

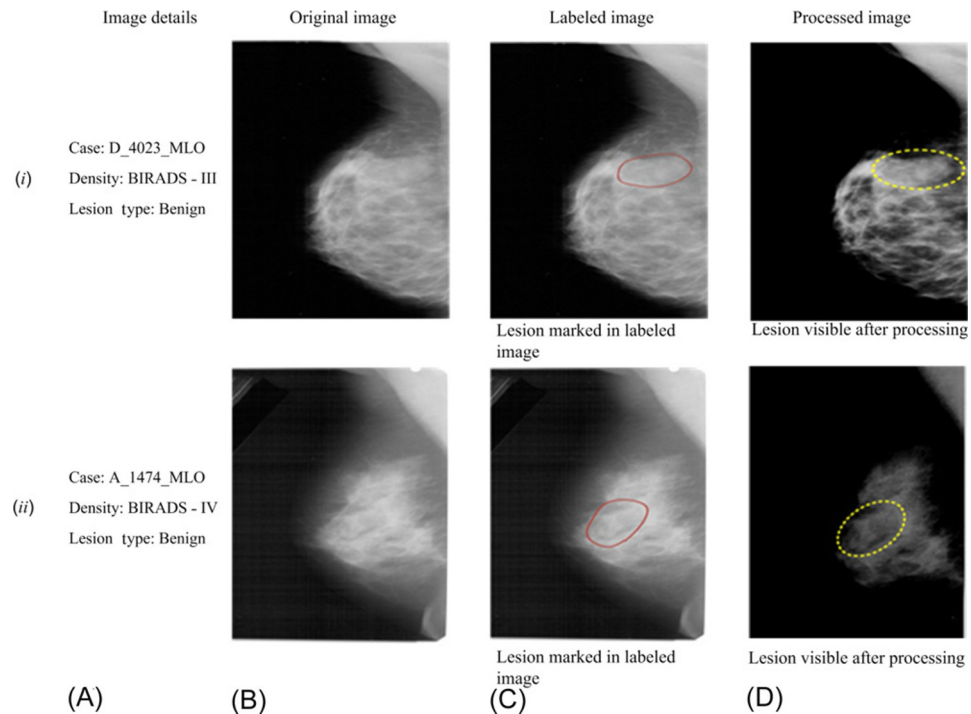
study recommends the use of the proposed computerized framework for breast tissue pattern characterization as given in [Fig. 21](#).

4 Conclusion and Future Scope

4.1 Conclusion

From the extensive experimentation carried out in this work it can be observed that (a) out of the four different ROI sizes higher classification accuracy values have been obtained with ROI size of 128×128 pixels using all the texture models for 4-class breast tissue pattern characterization as well as for 2-class breast tissue pattern characterization, (b) the highest accuracy of 79.5% has been achieved for 4-class breast tissue pattern characterization using GLCM texture features with interpixel distance “ d ” = 10 with SVM classifier, (c) the maximum accuracy of 91.2% has been achieved for 2-class breast tissue pattern characterization using Laws’ masks of kernel width 3 with SVM classifier.

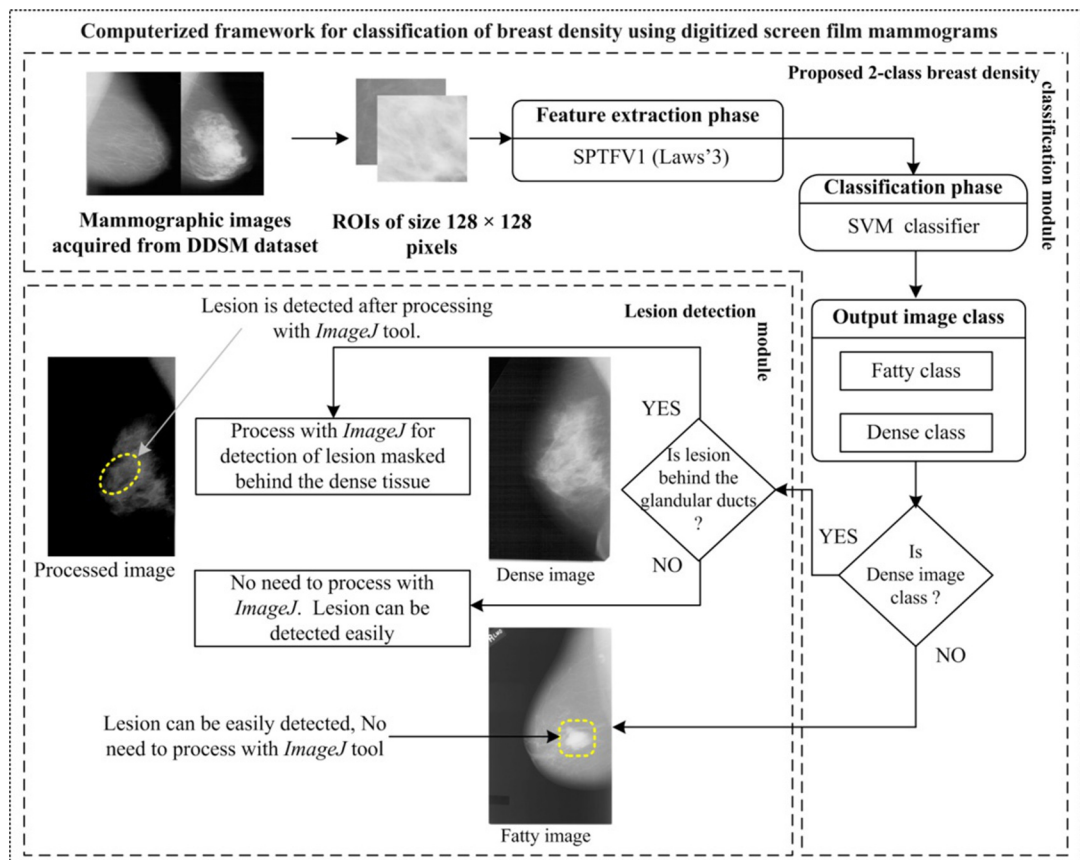
The present study recommends the use of the proposed computer assisted framework as shown in [Fig. 21](#) for characterization of 2-class breast tissue pattern using digitized SFMs in routine clinical practice.



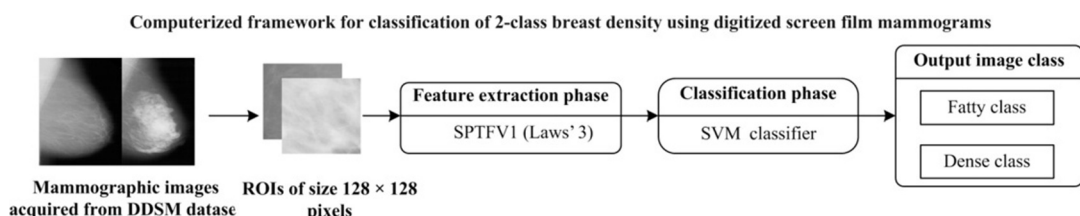
4.2 Future Scope

Till date, so many standard benchmark image database of digitized screen film mammograms (MIAS, DDSM) and full-field screen mammograms (InBreast) have been created with an objective of pooling it for research purpose. The present study has been carried out of digitized screen film mammograms; therefore it is not possible to compare similar studies on full-field screen mammograms. The following are the recommendations for the future work:

- (i) In the present work, ROIs are extracted manually. In future, texture based automatic segmentation algorithms can be developed to identify and extract ROIs automatically.
- (ii) In the proposed computerized framework, various texture feature computation have been carried out on raw images (i.e., without any sort of preprocessing i.e., denoising on the images). In future the effect of various denoising techniques on the mammographic images by various methods may be tested on the performance of proposed computerized framework.

**Fig. 20**

Computerized framework for detection of breast lesion using proposed computerized characterization framework. Note: If the prediction of 2-class breast tissue density characterization module is “dense” then the radiologist process the image (by adjusting brightness and contrast) using *ImageJ* module for detection of lesion masked behind the dense tissue.

**Fig. 21**

Proposed computer assisted framework for characterization of 2-class breast tissue pattern using digitized SFMs.

References

- [1] J. Ferlay, E. S-Foucher, J. Lortet-Tieulent, S. Rosso, J.W. Coebergh, H. Comber, D. Forman, F. Bray, Cancer incidence and mortality patterns in Europe: estimates for 40 countries in 2012, *Eur. J. Cancer* 49 (6) (2013) 1374–1403.
- [2] D.M. Parkin, L.M. Fernandez, Use of statistics to assess the global burden of breast cancer, *Breast* 12 (1) (2006) 70–80.
- [3] A. Papaevangelou, S. Chatzistergos, K.S. Nikita, G. Zografos, Breast density computerized analysis on digitized mammograms, *J. Hell. Stud.* 83 (3) (2011) 133–138.
- [4] J.J. Heine, M.J. Carton, C.G. Scott, An automated approach for estimation of breast density, *Cancer Epidemiol. Biomark. Prev.* 17 (11) (2008) 3090–3097.
- [5] Z. Huo, M.L. Giger, C.J. Vyborny, Computerized analysis of multiple-mammographic views: potential usefulness of special view mammograms in computer-aided diagnosis, *IEEE Trans. Med. Imaging* 20 (12) (2001) 1285–1292.
- [6] L. Yaghjyan, S.M. Pinney, M.C. Mahoney, A.R. Morton, J. Buckholz, Mammographic breast density assessment: a methods study, *Atlas J. Med. Biol. Sci.* 1 (1) (2011) 8–14.
- [7] K. Ganesan, U.R. Acharya, C.K. Chua, L.C. Min, T.K. Abraham, K.H. Ng, Computer aided breast cancer detection using mammograms: a review, *IEEE Trans. Biomed. Eng.* 6 (2013) 77–98.
- [8] I. Kumar, J. Virmani, H.S. Bhaduria, in: A review of breast density classification methods, Proceeding of 2nd International Conference on Computing for Sustainable Global Development ‘INDIACom—2015’: 1960–1967, 2015.
- [9] H. Wenda, A. Juette, E. Denton, A. Oliver, R. Martí, R. Zwiggelaar, A review on automatic mammographic density and parenchymal segmentation, *Int. J. Breast Cancer* 2015 (2015) 1–32.
- [10] G. Zhang, W. Wang, J. Moon, J.K. Pack, S. Jean, in: A review of breast tissue classification in mammograms, Proceedings of ACM Symposium on Research in Applied Computation, 2011, pp. 232–237.
- [11] M. Abdel-Nasser, H.A. Rashwan, D. Puig, A. Moreno, Analysis of tissue abnormality and breast density in mammographic images using a uniform local directional pattern, *Expert Syst. Appl.* 42 (24) (2015) 9499–9511.
- [12] E.U. Ekpo, U.P. Ujong, C. Mello-Thoms, M.F. McEntee, Assessment of inter-radiologist agreement regarding mammographic breast density classification using the fifth edition of the BI-RADS atlas, *Am. J. Roentgenol.* 206 (12) (2016) 1–5.
- [13] M. Kallenberg, K. Petersen, M. Nielsen, A.Y. Ng, D. Pengfei, C. Igel, M. V. Celine, K. Holland, N. Karssemeijer, M. Lillholm, Unsupervised deep learning applied to breast density segmentation and mammographic risk scoring, *IEEE Trans. Med. Imaging* 35 (5) (2016) 1322–1331.
- [14] A. Eng, Z. Gallant, Digital mammographic density and breast cancer risk a case-control study of six alternative density assessment methods, *Breast Cancer Res. Treat.* 16 (5) (2014) 439–451.
- [15] N.F. Boyd, L.J. Martin, M.J. Yaffe, S. Minkin, Mammographic density and breast cancer risk: Current understanding and future prospects, *Breast Cancer Res. Treat.* 13 (6) (2011) 223–234.
- [16] J.N. Wolfe, Risk for breast cancer development determined by mammographic parenchymal pattern, *Cancer* 37 (5) (1977) 2486–2492.
- [17] J.N. Wolfe, Breast patterns as an index of risk for developing breast cancer, *Am. J. Roentgenol.* 126 (6) (1976) 1130–1137.
- [18] E. Kang, E.J. Lee, M. Jang, S.M. Kim, Y. Kim, M. Chun, J.H. Tai, W. Han, S.W. Kim, J.H. Kim, Reliability computer-assisted breast density estimation: comparison of interactive thresholding, semi automated and fully automated methods, *Am. J. Roentgenol.* 207 (1) (2016) 1–9.
- [19] D.S. Al Mousa, P.C. Brennan, E.A. Ryan, W.B. Lee, J. Tan, C. Mello-Thomas, How mammographic breast density affects radiologists’ visual search patterns, *Acad. Radiol.* 21 (11) (2014) 1386–1393.
- [20] C. Colin, V. Prince, P.J. Valette, Can mammographic assessments lead to consider density as a risk factor for breast cancer, *Eur. J. Radiol.* 82 (3) (2013) 404–411.
- [21] E.A. Abdel-Gawad, O.A. Khalil, S.M. Ragae, Assessment of breast lesions using BI-RADS US lexicon in mammographically dense breasts (ACR categories 3 and 4) with histopathological correlation, *Egypt. J. Radiol. Nuclear Med.* 45 (2014) 1301–1307.

- [22] J. Tang, R.M. Rangayyan, J. Xu, I. Naqa, Y. Yang, Computer-aided detection and diagnosis of breast cancer with mammography: recent advances, *IEEE Trans. Inf. Technol. Biomed.* 13 (2) (2009) 236–251.
- [23] L. Hui, M.L. Giger, O.I. Olopade, A. Margolis, L. Lan, I. Bonta, Computerized texture analysis of mammographic parenchymal patterns of digitized mammograms, *Int. Congr. Ser.* 1268 (2004) 878–881.
- [24] D. Sacchetto, L. Morra, Mammographic density: comparison of visual assessment with fully automatic calculation on a multivendor dataset, *Eur. Radiol.* 26 (2016) 175–183.
- [25] L. Saba, N. Dey, A.S. Ashour, S. Samanta, S.S. Nath, S. Chakraborty, J.S. Suri, Automated stratification of liver disease in ultrasound: an online accurate feature classification paradigm, *Comput. Methods Prog. Biomed.* 130 (2016) 118–134.
- [26] A.S. Ashour, S. Samanta, N. Dey, N. Kausar, W.B. Abdessalemkarraa, A.E. Hassanien, Computed tomography image enhancement using cuckoo search: A log transform based approach, *J. Signal Inform. Proc.* 6 (03) (2015) 244.
- [27] N. Dey, A.S. Ashour, A.S. Ashour, A. Singh, Digital analysis of microscopic images in medicine, *J. Adv. Microsc. Res.* 10 (1) (2015) 1–13.
- [28] V. Rajnikanth, N. Dey, S.C. Satapathy, A.S. Ashour, An approach to examine magnetic resonance angiography based on Tsallis entropy and deformable snake model, *Futur. Gener. Comput. Syst.* 85 (2018) 160–172.
- [29] R. Thanki, S. Borra, N. Dey, A.S. Ashour, Medical imaging and its objective quality assessment: an introduction, in: *Classification in BioApps*, Springer, Cham, 2018, pp. 3–32.
- [30] N. Dey, A.S. Ashour, S. Borra (Eds.), *Classification in BioApps: Automation of Decision Making*, vol. 26, Springer, Cham, 2017.
- [31] P. Vidyasree, G. Madhavi, S. Viswanadharaju, S. Borra, A bio-application for accident victim identification using biometrics, in: *Classification in BioApps*, Springer, Cham, 2018, pp. 407–447.
- [32] A. Annavarapu, S. Borra, P. Kora, ECG signal dimensionality reduction-based atrial fibrillation detection, in: *Classification in BioApps*, Springer, Cham, 2018, pp. 383–406.
- [33] P. Kora, A. Annavarapu, S. Borra, ECG based myocardial infarction detection using different classification techniques, in: *Classification in BioApps*, Springer, Cham, 2018, pp. 57–77.
- [34] K. Bovis, S. Singh, in: Classification of mammographic breast density using a combined classifier paradigm, *Proceeding of Medical Image Understanding and Analysis ‘MIUA’ Conference*, Portsmouth, 2002, pp. 177–180.
- [35] A. Oliver, J. Freixenet, R. Zwiggelaar, in: Automatic classification of breast density, *Proceedings of the IEEE International Conference on Image Processing*, vol. 2, 2005, pp. 1258–1261.
- [36] A. Bosch, X. Munoz, A. Oliver, J. Marti, in: Modeling and classifying breast tissue density in mammograms, *Proceedings of the 2006 IEEE Computer Society Conference on Computer Vision and Pattern Recognition ‘CVPR’06’*, New York, vol. 2, 2006, pp. 1552–1558.
- [37] A. Oliver, J. Freixenet, R. Marti, J. Pont, E. Perez, E.R.E. Denton, R. Zwiggelaar, A novel breast tissue density classification methodology, *IEEE Trans. Inf. Technol. B* 12 (1) (2008) 55–65.
- [38] A. Oliver, X. Llado, E. Perez, E.R.E. Denton, J. Pont, J. Freixenet, J. Marti, A statistical approach for breast density segmentation, *J. Digit. Imaging* 23 (5) (2010) 527–537.
- [39] I. Kumar, H.S. Bhadauria, J. Virmani, Wavelet packet texture descriptors based four-class BIRADS breast tissue density classification, *Procedia Comput. Sci.* 70 (2015) 76–84.
- [40] I. Kumar, H.S. Bhadauria, J. Virmani, S. Thakur, A hybrid hierarchical framework for classification of breast density using digitized film screen mammograms, *Multimed Tools Appl.* 76 (18) (2017) 1–25.
- [41] I. Kumar, H.S. Bhadauria, J. Virmani, S. Thakur, A classification framework for the prediction of breast density using an ensemble of neural network classifiers, *Biocybern. Biomed. Eng.* 37 (1) (2017) 217–228.
- [42] I. Kumar, J. Virmani, H.S. Bhadauria, M.K. Panda, Classification of breast density patterns using PNN, NFC, and SVM classifiers, in: *Soft Computing Based Medical Image Analysis*, Academic Press, San Diego, United States, 2018, pp. 223–243.
- [43] Y. Qu, C. Shang, Q. Shen, Evolutionary fuzzy extreme learning machine for mammographic risk analysis, *Int. J. Fuzzy Syst.* 13 (4) (2011) 282–291.
- [44] Z. Chen, E. Denton, R. Zwiggelaar, in: Local feature based mammographic tissue pattern modeling and breast density classification, *Proceedings of 4th International Conference on Biomedical Engineering and Informatics*, Shanghai, 2011, pp. 351–355.

- [45] M. Mustra, M. Grgic, K. Delac, Breast density classification using multiple feature selection, *Automatika* 53 (4) (2012) 362–372.
- [46] V. Sharma, S. Singh, CFS-SMO based classification of breast density using multiple texture models, *Med. Biol. Eng. Comput.* 52 (6) (2014) 521–529.
- [47] V. Sharma, S. Singh, Automated classification of fatty and dense mammogram, *J. Med. Imaging Health Infor.* 5 (7) (2015) 520–526.
- [48] J. Virmani, Kriti, in: *Breast tissue density classification using wavelet-based texture descriptors*, Proceedings of the Second International Conference on Computer and Communication Technologies, Advances in Intelligent Systems and Computing, vol. 381, 2015, pp. 539–546.
- [49] Kriti, J. Virmani, N. Dey, V. Kumar, PCA-PNN and PCA-SVM based CAD systems for breast density classification, in: *Applications of Intelligent Optimization in Biology and Medicine*, vol. 96, Intelligent Systems Reference Library, Springer, Cham, 2016, pp. 159–180.
- [50] Kriti, J. Virmani, Breast density classification using Laws' mask texture features, *Int. J. Biomed. Eng. Technol.* 19 (3) (2015) 279–302.
- [51] Kriti, J. Virmani, S. Thakur, Application of statistical texture features for breast tissue density classification, in: *Image Feature Detectors and Descriptors*, Studies in Computational Intelligence, vol. 630, Springer, Cham, 2016, pp. 411–435.
- [52] Kriti, H. Kaur, J. Virmani, Evaluating the efficacy of multi-resolution texture features for prediction of breast density using mammographic images, in: *Hybrid Intelligence for Image Analysis and Understanding*, John Wiley and Sons Ltd., 2017, pp. 391–422.
- [53] Kriti, J. Virmani, R. Agarwal, Evaluating the efficacy of gabor features in the discrimination of breast density patterns using various classifiers, in: *Classification in BioApps*, Springer, Cham, 2018, pp. 105–131.
- [54] P. Miller, S. Astley, Classification of breast tissue by texture analysis, *BMVC91, Special Issue Image Vision Comput.* 10 (5) (1991) 277–282.
- [55] N. Karssemeijer, Automated classification of parenchymal patterns in mammograms, *Phys. Med. Biol.* 43 (2) (1998) 365–389.
- [56] S. Petroudi, T. Kadir, M. Brady, in: *Automatic classification of mammographic parenchymal patterns: a statistical approach*, Proceedings of the 25th Annual International Conference of the IEEE Engineering in Medicine and Biology Society, Cancun, Mexico, vol. 1, 2003, pp. 798–801.
- [57] N. Jamal, K.H. Ng, S. Ranganathan, L.K. Tan, in: *Comparison of computerized assessment of breast density with subjective BI-RADS classification and Tabar's pattern from two-view CR mammography*, World Congress on Medical Physics and Biomedical Engineering 2006, 2007, pp. 1405–1408.
- [58] Q. Liu, L. Liu, Y. Tan, J. Wang, X. Ma, H. Ni, Mammogram density estimation using sub-region classification, in: *Proceedings of 4th International Conference on Biomedical Engineering and Informatics 'BMEI'*, Shanghai, 2011, pp. 356–359.
- [59] A.D. Masmoudi, N.G.B. Ayed, D.S. Masmoudi, R. Abid, LBPV descriptors-based automatic ACR/BIRADS classification approach, *EURASIP J. Image Video Proc.* 1 (1) (2013) 1–9.
- [60] W. He, S. Harvey, A. Juette, E.R. Denton, R. Zwiggelaar, in: *Mammographic segmentation and density classification: a fractal inspired approach*, International Workshop on Digital Mammography, 2016, pp. 359–366.
- [61] H. Li, M.L. Giger, Z. Huo, O.I. Olopade, L. Lan, W.L. Weber, I. Bonta, Computerized analysis of mammographic parenchymal patterns for assessing breast cancer risk: Effect of ROI size and location, *Med. Phys.* 31 (3) (2004) 549–555.
- [62] M. Heath, K. Bowyer, D. Kopans, R. Moore, P.J. Kegelmeyer, The digital database for screening mammography, in: *Proc. Int. Workshop Digital Mammography*, 2000, pp. 212–218.
- [63] N.R. Mudigonda, R.M. Rangayyan, J.E.L. Desautels, Gradient and texture analysis for the classification of mammographic masses, *IEEE Trans. Med. Imaging* 19 (2000) 1032–1043.
- [64] N.R. Mudigonda, R.M. Rangayyan, J.E.L. Desautels, Detection of breast masses in mammograms by density slicing and texture flow-field analysis, *IEEE Trans. Med. Imaging* 20 (12) (2001) 1215–1227.
- [65] R. Haralick, K. Shanmugam, I. Dinstein, Textural feature for image classification, *IEEE Trans. Syst Man. Cyb.* 3 (6) (1973) 610–621.

- [66] R.M.M. Galloway, Texture analysis using gray level run lengths, *Comput. Vision Graph.* 4 (1975) 172–179.
- [67] A. Chu, C.M. Sehgal, J.F. Greenleaf, Use of gray value distribution of run lengths for texture analysis, *Pattern Recognit.* 11 (1990) 415–420.
- [68] B.V. Dasarathy, E.B. Holder, Image characterizations based on joint gray level-run length distributions, *Pattern Recognit.* 12 (1991) 497–502.
- [69] M. Vasantha, S. Bharathi, V. Dhamodharan, Medical image feature extraction, selection and classification, *Int. J. Eng. Sci. Technol.* 2 (2010) 2071–2076.
- [70] P. Mohanaiah, P. Sathyanarayananam, L. Gurukumar, Image texture feature extraction using GLCM approach, *Int. J. Sci. Res. Publ.* 3 (5) (2013) 1–5.
- [71] F. Albregtsen, Statistical texture measures computed from gray level run length matrices, *Image* 1 (1995) 3–8.
- [72] G. Castellano, L. Bonilha, L.M. Li, F. Cendes, Texture analysis of medical images, *Clin. Radiol.* 59 (2004) 1061–1069.
- [73] M. Amadasun, R. King, Textural features corresponding to textural properties, *IEEE Trans. Syst Man. Cyb.* 19 (1989) 1264–1274.
- [74] J.S. Weszka, C.R. Dyer, A. Rosenfeld, A comparative study of texture measures for terrain classification, *IEEE Trans. Syst Man. Cyb.* 6 (4) (1976) 269–285.
- [75] J.K. Kim, H.W. Park, Statistical textural features for detection of microcalcifications in digitized mammograms, *IEEE Trans. Med. Imaging* 18 (3) (1999) 231–238.
- [76] K.I. Laws, Rapid texture identification, *SPIE Proc. Semin. Image Process Missile Guid.* 238 (1980) 376–380.
- [77] C. Lee, S.H. Chen, Gabor wavelets and SVM classifier for liver diseases classification from CT images *Proceedings of IEEE International Conference on Systems, Man, and Cybernetics* (2006) pp. 548–552.
- [78] M. Sharma, M. Markou, S. Singh, in: Evaluation of texture methods for image analysis, *Proceedings of the Seventh Australian and New Zealand Intelligent Information Systems Conference, 2001*, , pp. 117–121.
- [79] J. Virmani, V. Kumar, N. Kalra, N. Khandelwal, Neural network ensemble based CAD system for focal liver lesions from B-mode ultrasound, *J. Digit. Imaging* 27 (2014) 520–537.
- [80] C.C. Chang, C.J. Lin, LIBSVM, A library of support vector machines, Available from: <http://www.csie.ntu.edu.tw/~cjlin/libsvm>, 2012.
- [81] A.J. Viera, J.M. Garrett, Understanding interobserver agreement: the kappa statistic, *Fam. Med.* 37 (5) (2005) 360–363.
- [82] W.S. Rasband, ImageJ, U. S. National Institutes of Health, Bethesda, Maryland, USA, Available from <https://imagej.nih.gov/ij/>, 1997–2018.
- [83] M.D. Abramoff, P.J. Magalhaes, Image processing with ImageJ, *Biophotonics* (2004) 1–7.

Further Reading

- [84] A.E. Hassanien, N.E. Bendary, M. Kudelka, V. Snasel, in: Breast cancer detection and classification using support vector machines and pulse coupled neural network, *Proceedings of 3rd International Conference on Intelligent Human Computer Interaction ‘IHCI 2011’*, 2011, pp. 269–279.
- [85] A.T. Azar, S.A. El-Said, Performance analysis of support vector machine classifiers in breast cancer mammography recognition, *Neural Comput. Appl.* 24 (2014) 1163–1177.